Volume Rendering of Dense B-Scan Optical Coherence Tomography Angiography to Evaluate the Connectivity of Macular Blood Flow

Diogo Cabral,[1–3] Telmo Pereira,[2] Gerardo Ledesma-Gil,[1] Catarina Rodrigues,[2,3] Florence Coscas,[4,5] David Sarraf,[6] and K. Bailey Freund[1,7]

[1]Vitreous, Retina, Macula Consultants of New York, New York, New York, United States
[2]CEDOC, NOVA Medical School I Faculdade de Ciências Médicas, Universidade NOVA de Lisboa, Lisbon, Portugal
[3]Instituto de Oftalmologia Dr. Gama Pinto, Lisbon, Portugal
[4]Centre Ophtalmologique de l'Odéon, Paris, France
[5]Department of Ophthalmology, Centre Hospitalier Intercommunal de Creteil, University Paris Est Creteil XII, Créteil, France
[6]Retina Division, Stein Eye Institute, University of California, Los Angeles, Los Angeles, California, United States
[7]Department of Ophthalmology, NYU Grossman School of Medicine, New York, New York, United States

Correspondence: K. Bailey Freund, Vitreous, Retina, Macula Consultants of New York, 950 3rd Avenue, 3rd Floor, New York, NY 10022, USA; kbfreund@gmail.com.

Received: April 15, 2020
Accepted: May 19, 2020
Published: June 19, 2020

Citation: Cabral D, Pereira T, Ledesma-Gil G, et al. Volume rendering of dense B-scan optical coherence tomography angiography to evaluate the connectivity of macular blood flow. *Invest Ophthalmol Vis Sci.* 2020;61(6):44. https://doi.org/10.1167/iovs.61.6.44

Purpose. To characterize macular blood flow connectivity using volume rendering of dense B-scan (DB) optical coherence tomography angiography (OCTA) data.

Methods. This was a prospective, cross-sectional, observational study. DB OCTA perifoveal scans were performed on healthy subjects using the Spectralis HRA+OCT2. A volumetric projection artifact removal algorithm and customized filters were applied to raw OCTA voxel data. Volume rendering was performed using a workflow on Imaris 9.5 software. Vascular graphs were obtained from angiographic data using the algorithm threshold-loops. Superficial arteries and veins were identified from color fundus photographs and connections between adjacent arteries and veins displayed using the shortest path algorithm. Connective pathway locations were analyzed with cross-sectional OCT and OCTA to determine their course through the superficial vascular complex (SVC) and the deep vascular complex (DVC).

Results. Fourteen eyes from seven subjects (mean age: 28 ± 5 years; 3 women) were included in this analysis. One hundred and twenty-six vascular connections were analyzed. In all cases, the shortest path connections between superficial arteries and veins coursed through the DVC. We did not identify shortest path connections confined to the SVC.

Conclusions. Volumetric analysis of vascular connectivity supports a predominantly in-series arrangement of blood flow between the SVC and DVC within the human perifoveal macula.

Keywords: optical coherence tomography, DB OCTA, volume rendering, shortest path algorithm, vascular graphs

Macular vasculature consists of an intricate mesh of fine capillaries. Disruption of the normal organization is associated with ischemia and retinal dysfunction. Therefore understanding blood flow organization is essential to study macular vascular diseases.

Early histologic work identified two inner and two outer capillary beds in nonhuman primates and human donor tissue.[1–4] Using projection-resolved optical coherence tomography angiography (OCTA) and structural optical coherence tomography (OCT), Campbell et al.[5] developed a system for segmenting the retinal circulation into two complexes (superficial vascular complex [SVC] and deep vascular complex [DVC]) and four plexuses (radial peripapillary, superficial [SCP], intermediate [ICP], and deep capillary plexus [DCP]). In the macula, the DVC can be divided into the ICP and the DCP. Applying an anatomically accurate segmentation to structural OCT, Gattoussi and Freund[6] validated the presence of two plexuses with distinct vascular patterns bracketing the inner nuclear layer (INL) in the central macula (ICP and DCP).

Our current understanding of vascular connectivity and how blood flows through this circuit originates from various studies, including animal models,[7–9] OCTA investigations,[5,10,11] and structure-function relationships,[12–15] with arguments favoring distinct types of blood flow organization. Using en face OCTA and OCT B-scans, Nesper and Fawzi[10] found an independent arteriolar supply to the DCP and draining venules for each of the three capillary plexuses in the parafovea, supporting a hybrid model arrangement of macular blood flow, with both parallel and serial components.[5] Analyzing 16 perfusion-labeled human donor eyes, An et al.[16] found no direct arterial supply to the DCP, and

concluded that all arterial supply to the DCP originates from the ICP.

Using en face OCT, OCTA segmentation, and color-coded volume renderings, Freund et al.[15] showed that all of the 101 collateral vessels associated with branch or hemispheric retinal vein occlusion coursed through the DVC. These authors suggested that an absence of connections at the SCP indicated that the retinal capillary plexuses were arranged more in series than in parallel. This model agrees with imaging findings of paracentral acute middle maculopathy (PAMM) lesions, whereby deep perivenous retinal tissue would be vulnerable to ischemia due to its distal location with respect to arterial supply.[13–15,17] However, none of these studies have been exempt of limitations, and connectivity of the retinal capillary plexuses is still incompletely understood.

Volumetric acquisition of OCT enables the construct of a vascular graph from angiographic data and the capability to analyze it simultaneously with structural OCT.[18] Qualitative analysis of vascular graphs has been conducted in patients with various vascular diseases.[19–21] With the evolution of OCTA technology, Freund et al.[22] described the method of dense B-scan (DB) OCTA that enables evaluation of retinal capillary blood flow at higher resolution than conventional acquisitions. Advances in projection artifact removal (PAR) have enabled volumetric algorithms (three-dimensional [3D] PAR) that help preserve connections between the retinal plexuses better than prior two-dimensional PAR algorithms. The aim of our study was to characterize macular blood flow network connectivity using vascular graphs obtained after volumetric rendering of DB OCTA and application of 3D PAR.

Methods

Study Design and Setting

This was a prospective, observational study of healthy subjects observed in October 2019 at Vitreous, Retina, and Macula consultants center (New York, NY, USA). This study was approved by the institutional review board committee of the western institutional review board and was conducted in accordance with the tenets of the Declaration of Helsinki (1964) and complied with the Health Insurance Portability and Accountability Act of 1996. All enrolled patients gave their written consent at the time of recruitment.

Participants and Image Acquisition

All subjects had no history of ocular disease or systemic diseases affecting the retinal vasculature. All eyes underwent high-resolution confocal color fundus photography (EIDON AF; CenterVue, Padova, Italy) and one DB OCTA in either the superior or the inferior perifoveal region (10° × 3°) using the Spectralis HRA+OCT2 (Heidelberg Engineering, Heidelberg, Germany). DB OCTA acquisitions were acquired as previously described.[22] Each OCTA volume consisted of 500 B-scans with an interscan distance of 1.79 µm nominal spacing. Seven repeated OCT B-scans at each tissue location were used by the full-spectrum probabilistic OCTA algorithm to determine the presence or absence of flow at each voxel. An investigational version of the Heidelberg Eye Explorer (HEYEX ver. 6.12.4.710; Heidelberg Engineering) was used for image acquisition, processing, and post-processing of OCTA data. The onboard volumetric PAR algorithm ("3D PAR vessel strong") that performs 3D vessel shape estimation in the volume and only operates to remove their projection tails was employed to remove projection artifacts. Raw (floating point) data were exported as .VOL file for further analysis.

Image Analysis

Image processing and analysis was done using a code designed in MATLAB version R2019b (The MathWorks Inc., Natick, MA, USA). Structural OCT and OCTA data were extracted from raw data following the manufacturer's instructions. OCTA data were then interpolated 10 times on the z-axis and a linear quadratic estimation (Kalman filter) employing an initial noise variance estimate of 0.05 and a gain of 0.8, as previously described.[23] After this step, Gaussian smoothing was performed on the images using a Gaussian filter of radius 0.8 σ (which corresponds to the standard deviation of the Gaussian).

Eleven structural OCT boundaries were segmented using the HEYEX software. The scans were manually checked for correct segmentation of the inner limiting membrane (ILM), the ganglion cell layer (GCL), the inner plexiform layer (IPL), the INL, and the outer plexiform layer (OPL). The SVC was defined as crossing the nerve fiber layer, GCL and superficial IPLs, as previously described.[5,24] Automated segmentation parameters included the ILM and a 17-µm offset anterior to the IPL [IPL (-) derived from automatic segmentation]. The DVC was defined as bracketing the deeper GCL, the deeper part of the relatively thin IPL, and the synaptic portion of the OPL.[5,15] Automated segmentation parameters included IPL (-) and the OPL boundary. Figure 1 shows the distinct separation and morphology of the SVC and DVC using DB OCTA data.

Volume Rendering and Rendering Quality Assessment

Vascular casts from OCTA data were issued using a workflow on Imaris v9.5 (Bitplane, Andor Technology plc. Zurich, Switzerland). Data were segmented using the surfaces tool with 7-µm surfaces detail and local contrast threshold of 10 µm. The segmented surface mask was used in the filament tracer tool to reconstruct the 3D volumetric data. The algorithm *threshold loops* option was selected with feature preprocessing of 10 µm and a branch length to trunk ratio of 2. After vascular casts construction, data were visualized using the Imaris 3D viewer and exported to MATLAB using the Imaris XTensions module for quality assessment.

Quality assessment was performed to validate the rendering quality when compared with the ground truth OCTA data. Ground truth data were obtained using the MATLAB imbinarize function, including the adaptative threshold option and sensitivity of 0.01. The filament data exported from Imaris was skeletonized in 3D using the Skeleton3D algorithm.[25] The overlap of the resultant datasets (ground truth and filament data) were compared with the total volume of the ground truth data originating the final quality ratio. The process for evaluating rendering quality is depicted in Supplementary Figure S1.

Evaluation of Connectivity

En face OCTA superficial slabs were registered with confocal color fundus photographs using the plugin "landmark correspondences" of Fiji (ImageJ v1.52p; National Institutes

Investigative Ophthalmology & Visual Science

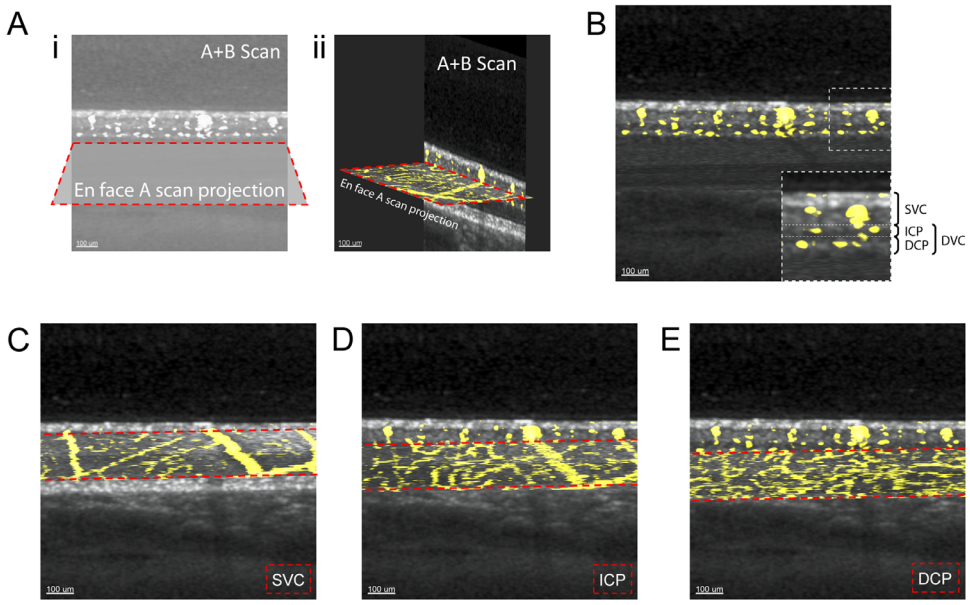

Figure 1. Structural OCT and OCTA after volumetric PAR demonstrating distinct separation and morphology of the SVC and DVC. (**A**) Diagram illustrating the arrangement of orthogonal cross-sections: cross-section on the XZ axis demonstrates structural B-scan and A-scan signal, and cross-section on the XY axis (*red dashed lines*) demonstrates A-scan signal according to the level spanned; (**B**) A- and B-scan demonstrates OCTA signal in three well-defined layers. *Inset* shows a magnified view of an A- + B-scan region (*dashed line*) with identification of the two complexes of retinal circulation (SVC and DVC). In the macula, the DVC can be divided into the ICP and the DCP. (**C, D, E**) Cross-section at the SVC, ICP, and DCP levels, respectively. En face OCTA depicts different morphologic patterns within these plexuses.

of Health, Bethesda, MD, USA)[26] and arterioles and venules were colored accordingly in the vascular graph.[27] Pathway analysis was conducted using Imaris. Three pairs of adjacent arterioles and venules were considered per vascular graph. The departing point was set in the arteriole of interest, the arrival point was set in the vein of interest, and the "path" option was selected to track the pathways between these nodes. For this calculation, the software employs the shortest path problem algorithm: an algorithm that finds the shortest paths between nodes on a graph, which represent, in this case, connections between superficial arteries and veins. Connections were highlighted for further analysis.

Results

Fourteen eyes from seven subjects were evaluated. The mean age was 28 years (± 5 years) and three study patients were women. The mean quality ratio obtained from the comparison between vascular casts skeleton and ground truth data were 86.9% ± 1.8%.

We evaluated 126 shortest path connections between the largest superficial arteries and veins. In all cases, the shortest path connections coursed through the DVC (ICP + DCP). We did not identify any shortest path connections confined to the SVC. Superficial arterioles connected more commonly to the ICP. At the ICP, shortest paths continued either to the DCP or ascended to a vein at the level of the SVC. The DCP received most connections from the ICP; however, some shortest pathways connected directly with the SVC. Some pathways coursing through the DCP and then ascending to veins at the level of the SVC were joined by other connections coursing through the ICP (Fig. 2). We observed that pathways frequently bifurcated at the ICP, with one path connecting to a collecting venule at the level of the SVC, and a second path coursing through the DCP before ascending to a collecting venule at the level of the SVC (Fig. 3). Finally, we observed that connecting segments between the DCP and veins at the level of the SVC originated within an arrangement of DCP capillaries resembling a vortex (Fig. 4).

Following these observations, we depict in Figure 5 and Supplementary Video vascular graphs colored according to the connections of each vascular segment. Segments connecting to the major superficial artery (arterioles) were tinted with red, vascular segments connecting to the major venule (venules) were tinted with blue, and capillaries between arterioles and venules were tinted with green. The shortest pathways are highlighted in white and their progression through the DVC is shown using slices of the structural OCT with projection of OCTA signal. Supplementary Figure S2 shows schematic representations of different types of blood flow organization, including the earlier-mentioned findings of a serial connectivity between SVC and DVC.

Discussion

In this study, we applied a novel approach using volume rendering of DB OCTA data and an automated shortest path algorithm to explore the connectivity of macular blood flow. We evaluated 126 shortest path connections between superficial arteries and veins from the parafovea of seven healthy subjects (14 eyes). Each connection we evaluated coursed through the DVC (ICP + DCP). Our results suggest that any arteriovenous connection confined to the SVC would be longer than arteriovenous connections coursing through the DVC. We found that most connections to the DCP course through the ICP, with fewer direct connections

Investigative Ophthalmology & Visual Science

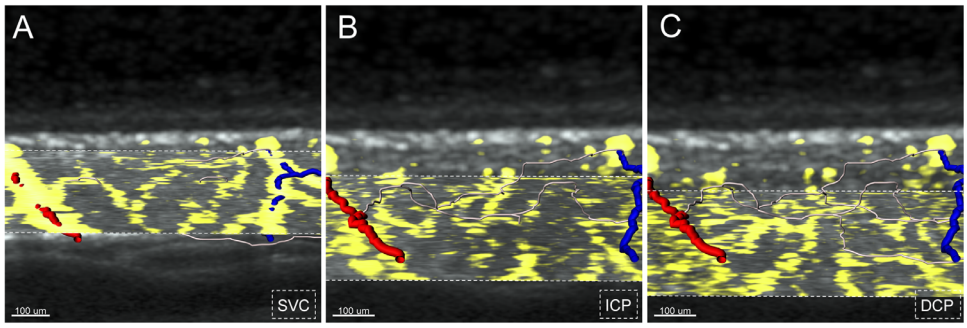

Figure 2. Structural OCT and OCTA with shortest pathways between adjacent superficial major artery and vein. (**A**) En face OCTA spanning the SVC (*white dashed lines*): shortest paths (*white*) departing from the artery (*red*) dive into the ICP, without any major venous outflow connections at this level. (**B, C**) Depict en face OCTA of the DVC: shortest paths cross the ICP (**B**) or the DCP (**C**) before ascending to the venular side of blood flow.

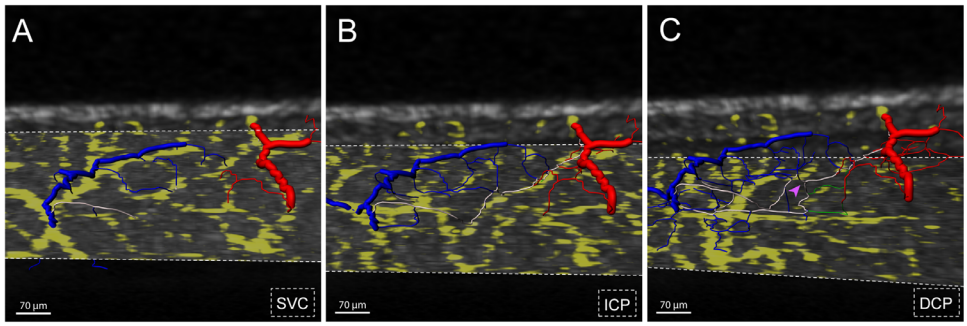

Figure 3. Structural OCT and OCTA superimposed with a vascular graph colored according to the connections of each vascular segment. (**A**) Cross-sections at the SVC (*white dashed lines*): we observe absence of major connections between arterioles (*red*) and venules (*blue*); (**B**) cross-sections at the ICP level (*white dashed lines*): we observe a major arteriovenous connection crossing this level. The connection is highlighted with *white* as it represents a shortest pathway between major superficial artery and vein; (**C**) cross-section at retinal DCP: we observe a bifurcation (*magenta arrow head*) of the shortest path at the ICP level, with two branches connecting to the SVC: a branch ascending through the ICP and a branch passing through the DCP. Both connections are highlighted with *white* as they represent shortest pathways between superficial artery and vein.

from the SVC to the DCP. Our finding that most shortest pathways course in series through the ICP and DCP before ascending to veins at the level of the SVC supports other investigators descriptions of the DCP playing a major role in macular venous drainage.[14,15,17,27] We also observed that shortest paths often bifurcated within the ICP, with one path connecting to a collecting venule, and a second coursing through the DCP before ascending to a vein at the level of the SVC. Finally, we found that pathways ascending from the DCP to join a vein in the SVC originate from DCP vortices, in agreement with previous OCTA[11,27] and histologic studies.[4,7] Taken together, our findings support

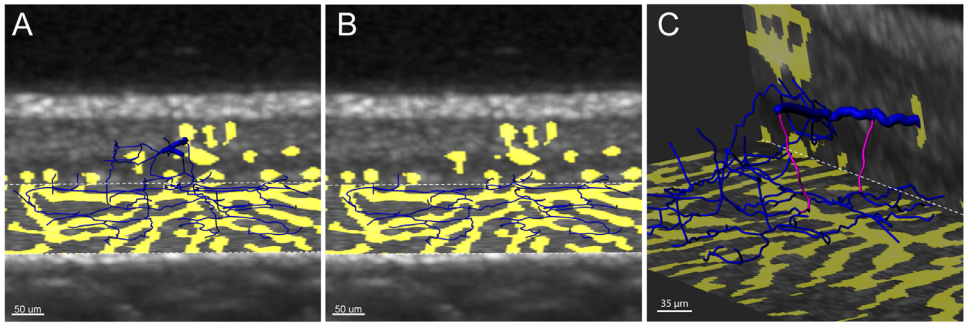

Figure 4. Structural OCT and OCTA depicting DCP morphology and connections to the superficial plexus. (**A**) Cross-sectional structural OCT, en face OCTA of the DCP (*white dashed lines*), and volumetric reconstruction of the vascular segments above a main superficial vein; (**B**) cross-section at the DCP (*white dashed lines*) highlights a vortex-like arrangement of vascular segments that converge toward central collecting channels; (**C**) detail of the volumetric reconstruction depicting two collecting channels (*magenta*) arising at the convergence of DCP vascular segments and connecting the DCP to a main venous channel located above.

Investigative Ophthalmology & Visual Science

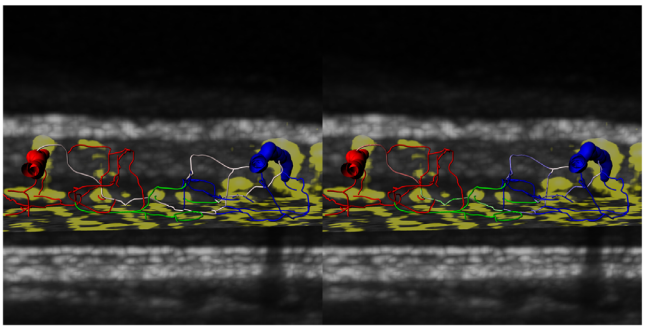

Figure 5. Structural OCT and OCTA with the shortest pathways between adjacent superficial artery and vein. Stereopair image. Superficial artery and vein were colored following color fundus photographs. Vascular graphs obtained after filament tracing were colored artificially according to the connections of each vascular segment: arterioles were tinted with *red*, venules with *blue*, and capillaries with *green*. The shortest pathway between superficial artery and vein is highlighted with *white*. We observe that the preferential pathway between major artery and vein percolates through the DVC, with absence of shortest pathways at the level of the SVC.

prior structural and functional inferences that an in-series arrangement of arterial flow predominates between the SVC and DVC in the human perifoveal macula.[13–15,7]

Other investigators have proposed a parallel model of perifoveal macular blood flow, either as strict capillary "hammocks" with all arteriovenous connections confined to separate vascular plexuses,[5] or a hybrid with a predominantly parallel model, with a limited number of vertical connections between plexuses.[10] The parallel models postulate that each plexus integrate distinct neurovascular units, with independent arterial inflow and venous outflow. This connectivity model was proposed based on en face OCTA studies analyzed with manual tracing of the connection between capillaries in SVC, ICP, and DCP, and feeding arteries and/or draining veins in the SVC. Although we did not demonstrate arteriovenous connections confined to the SVC using a shortest pathway approach, this does not mean a complete absence of those connections. We believe our results support those of authors who have concluded that a hybrid model for perifoveal macular blood flow exists in which blood flow percolates preferentially in a serial organization.[8]

Our findings provide important insight for the understanding of common vascular diseases of the macula. In cases of retinal venous occlusion (RVO), several authors have noted that collateral formation develops within the deep layers, both in rodent models[28] and in humans.[15] Our work supports that the pathway for physiologic venous outflow is similar to that observed in pathologic adaptation to venous outflow obstruction. Therefore in cases of increased venous pressure we would observe dilation of the shortest pathways connecting to SVC venules. However, we acknowledge that factors other than vessel length could be implicated, including reduced resistance in the DVC and potential channels that cross the horizontal raphe in the DCP, as suggested by other investigators.[10] Ghasemi Falavarjani et al.[14] and Bakhoum et al.[17] described a spectrum and progression of PAMM lesions in eyes with RVO. The authors hypothesized that venous outflow obstruction resulting in delayed flow through the vascular beds arranged in-series would result in greater ischemic damage to tissue surrounding the most distal vessels. In our study, we found that serial arrangements of the shortest pathways connected SVC to ICP, with many pathways traversing the DCP before ascending to the venous collecting channels. These results support the hypothesis that a prolonged vascular transit time would cause more ischemia in the deeper perivenular tissue. Also, Au et al.[29] described a series of eyes with macular telangiectasia type 2 presenting with spontaneous intraretinal hemorrhage confined to the Henle fiber layer, but lacking evidence of macular neovascularization. The authors reasoned that structural weakness in DVC capillaries could result in deep retinal hemorrhage with sudden increases in venous hydrostatic pressure. This mechanism may also explain other causes of Henle fiber layer hemorrhage associated with local (e.g. RVO) and systemic venous disorders (e.g., Tersons) that result in bleeding at the level of the DCP.[30] Our shortest pathways analysis finding of the DVC more distal location with direct connections to veins in the SVC supports their hypothesis.

Strengths of our study included the use of an automated image analysis protocol using a computer algorithm that did not rely on manual tracing to select the shortest paths. Additionally, the use of DB OCTA data provided higher resolution images with a higher signal-to-noise ratio than standard OCTA acquisitions using commercial spectral domain and swept source OCT devices. We also performed 3D analyses of data after employing a volumetric PAR algorithm, unlike some investigators who used slab-subtraction algorithms for PAR. Our image analysis protocol showed strong reliability, which enables this technique of volumetric analysis to be tested on data from other patient cohorts.

Limitations included the inclusion of only healthy subjects, which limits inferences regarding pathological states. We also acknowledge that although volume-based PAR should not inadvertently remove connections in the SVC, it could eliminate connections in the deep layers. Therefore our work could underrepresent the connectivity between the ICP and DCP and between the SCP and DCP. Moreover, employing a shortest path algorithm to track connections between arteries and veins may have overrepresented connectivity through the ICP, as the distance between vessels connecting the SVC and ICP would likely be shorter than connections between vessels in the SVC and DCP. Although the shortest pathway may also be considered a more physiologic approach to address connectivity, we have accounted for these limitations while interpreting the results. Finally, it is possible for capillary segments to exist that are not detected with current OCTA technology. Averaging the signal of multiple high-resolution acquisitions would increase the signal-to-noise ratio and could possibly render low flow and/or intermittent flow within SVC connections, if present, traceable. Future studies will be needed to address this subject.

Conclusions

A shortest pathway analysis of connectivity between superficial arteries and veins within the perifoveal macula demonstrated a preferential coursing through the DVC. Our findings support a predominantly serial arrangement of this retinal vascular system in which most venous drainage originates in the DVC.

Investigative Ophthalmology & Visual Science

Acknowledgments

The authors thank David Huang, MD, PhD, and Joseph Carroll, PhD, for providing the idea of using circuit diagrams to demonstrate retinal blood flow connectivity; Michel Teussink, PhD, medical science liaison at Heidelberg Engineering, Inc. (Heidelberg, Germany), for providing technical specifications for the Spectralis HRA+OCT2 and the dense B-scan optical coherence tomography angiography module described in the Methods section.

Supported by The Macula Foundation, Inc. (KBF), New York, New York, USA, and the Research to Prevent Blindness Inc. (DS), New York, New York, USA.

Disclosure: **D. Cabral**, None; **T. Pereira**, None; **G. Ledesma-Gil**, None; **C. Rodrigues**, None; **F. Coscas**, None; **D. Sarraf**, Amgen (C, F), Bayer (C), Genentech (C, F), Optovue (C, F), Novartis (S), Heidelberg Engineering (F), Regeneron (F), Topcon (F); **K.B. Freund**, Genentech (C), Optovue (C), Zeiss (C), Heidelberg Engineering (C), Allergan (C), Bayer (C), Novartis (C), Genentech/Roche (F)

References

1. Tan PEZ, Yu PK, Balaratnasingam C, et al. Quantitative confocal imaging of the retinal microvasculature in the human retina. *Invest Ophthalmol Vis Sci*. 2012;53:5728–5736.
2. Henkind P. Radial peripapillary capillaries of the retina. I. Anatomy: human and comparative. *Br J Ophthalmol*. 1967;51:115–123.
3. Foreman DM, Bagley S, Moore J, Ireland GW, Mcleod D, Boulton ME. Three dimensional analysis of the retinal vasculature using immunofluorescent staining and confocal laser scanning microscopy. *Br J Ophthalmol*. 1996;80:246–251.
4. Snodderly DM, Weinhaus RS, Choi JC. Neural-vascular relationships in central retina of macaque monkeys (*Macaca fascicularis*). *J Neurosci*. 1992;12:1169–1193.
5. Campbell JP, Zhang M, Hwang TS, et al. Detailed vascular anatomy of the human retina by projection-resolved optical coherence tomography angiography. *Sci Rep*. 2017;7:42201.
6. Gattoussi S, Freund KB. Correlating structural and angiographic optical coherence tomography in the intermediate and deep retinal capillary plexuses. *Exp Eye Res*. 2017;165:96–98.
7. Fouquet S, Vacca O, Sennlaub F, Paques M. The 3D retinal capillary circulation in pigs reveals a predominant serial organization. *Invest Ophthalmol Vis Sci*. 2017;58:5754–5763.
8. Pi S, Camino A, Wei X, et al. Rodent retinal circulation organization and oxygen metabolism revealed by visible-light optical coherence tomography. *Biomed Opt Express*. 2018;9:5851.
9. Paques M, Tadayoni R, Sercombe R, et al. Structural and hemodynamic analysis of the mouse retinal microcirculation. *Invest Ophthalmol Vis Sci*. 2003;44:4960–4967.
10. Nesper PL, Fawzi AA. Human parafoveal capillary vascular anatomy and connectivity revealed by optical coherence tomography angiography. *Invest Ophthalmol Vis Sci*. 2018;59:3858–3867.
11. Bonnin S, Mané V, Couturier A, et al. New insight into the macular deep vascular plexus imaged by optical coherence tomography angiography. *Retina*. 2015;35:2347–2352.
12. Nesper PL, Lee HE, Fayed AE, Schwartz GW, Yu F, Fawzi AA. Hemodynamic response of the three macular capillary plexuses in dark adaptation and flicker stimulation using optical coherence tomography angiography. *Invest Ophthalmol Vis Sci*. 2019;60:694–703.
13. Garrity ST, Paques M, Gaudric A, Freund KB, Sarraf D. Considerations in the understanding of venous outflow in the retinal capillary plexus. *Retina*. 2017;37:1809–1812.
14. Ghasemi Falavarjani K, Phasukkijwatana N, Freund KB, et al. En face optical coherence tomography analysis to assess the spectrum of perivenular ischemia and paracentral acute middle maculopathy in retinal vein occlusion. *Am J Ophthalmol*. 2017;177:131–138.
15. Freund KB, Sarraf D, Leong BCS, Garrity ST, Vupparaboina KK, Dansingani KK. Association of optical coherence tomography angiography of collaterals in retinal vein occlusion with major venous outflow through the deep vascular complex. *JAMA Ophthalmol*. 2018;136:1262–1270.
16. An D, Yu P, Freund KB, Dao-Yi Y , Balaratnasingam C. Three-dimensional characterization of the normal human parafoveal microvasculature using structural criteria and high-resolution confocal microscopy. *Invest Ophthalmol Vis Sci*. In press.
17. Bakhoum MF, Freund KB, Dolz-Marco R, et al. Paracentral acute middle maculopathy and the ischemic cascade associated with retinal vascular occlusion. *Am J Ophthalmol*. 2018;195:143–153.
18. Spaide RF. Volume-rendered angiographic and structural optical coherence tomography. *Retina*. 2015;35:2181–2187.
19. Spaide RF. Volume-rendered optical coherence tomography of diabetic retinopathy pilot study. *Am J Ophthalmol*. 2015;160:1200–1210.
20. Spaide RF, Klancnik JM, Cooney MJ, et al. Volume-rendering optical coherence tomography angiography of macular telangiectasia type 2. *Ophthalmology*. 2015;122:2261–2269.
21. Spaide RF. Volume-rendered optical coherence tomography of retinal vein occlusion pilot study. *Am J Ophthalmol*. 2016;165:133–144.
22. Freund KB, Gattoussi S, Leong BCS. Dense B-scan optical coherence tomography angiography. *Am J Ophthalmol*. 2018;190:78–88.
23. Kalman RE. A new approach to linear filtering and prediction problems. *J Fluids Eng*. 1960;82:35–45.
24. Spaide RF, Curcio CA. Evaluation of segmentation of the superficial and deep vascular layers of the retina by optical coherence tomography angiography instruments in normal eyes. *JAMA Ophthalmol*. 2017;135:259–262.
25. Kollmannsberger P, Kerschnitzki M, Repp F, Wagermaier W, Weinkamer R, Fratzl P. The small world of osteocytes: connectomics of the lacuno-canalicular network in bone. *New J Phys*. 2017;19:073019.
26. Schindelin J, Arganda-Carreras I, Frise E, et al. Fiji: an open-source platform for biological-image analysis. *Nat Methods*. 2012;9:676–682.
27. Xu X, Yannuzzi NA, Fernández-Avellaneda P, et al. Differentiating veins from arteries on optical coherence tomography angiography by identifying deep capillary plexus vortices. *Am J Ophthalmol*. 2019;207:363–372.
28. Genevois O, Paques M, Simonutti M, et al. Microvascular remodeling after occlusion-recanalization of a branch retinal vein in rats. *Invest Ophthalmol Vis Sci*. 2004;45:594–600.
29. Au A, Hou K, Baumal CR, Sarraf D. Radial hemorrhage in Henle layer in macular telangiectasia type 2. *JAMA Ophthalmol*. 2018;136:1182–1185.
30. Baumal CR, Sarraf D, Bryant T, et al. Henle fiber layer hemorrhage: clinical features and pathogenesis. *Br J Ophthalmol*. Published Online First: 06 May 2020.

Investigative Ophthalmology & Visual Science

Supplementary Material

Supplemental Video. Volume rendering of structural OCT and OCTA with 3D tracing of the shortest pathways between an adjacent superficial artery and vein. A volume rendering of OCTA blood flow signal (*yellow*) volume rendering is shown. A superficial artery and vein in a region of interest were colored following color fundus photographs. Vascular segmentation obtained after filament tracing (*green*) is depicted. Segments were color- coded according to the connections of each vascular segment: connections with superficial arterioles were colored *red*, connections with superficial venules with *blue*, and capillaries between those connections with *green*. The shortest pathways between superficial artery and vein are highlighted with *white*. We observed after several slices of structural OCT with projection of blood flow signal the preferential pathway between major artery and vein passes through the DVC, with an absence of shortest pathways confined to the SVC.

Investigative Ophthalmology & Visual Science